Interactions, Behavior, And Stability of Fluorenone inside Zeolite Nanochannels

Ettore Fois,*,† Gloria Tabacchi,† and Gion Calzaferri‡

Department of Chemical and Environmental Sciences and INSTM, University of Insubria, Via Lucini 3, I-22100 Como, Italy, and Department of Chemistry and Biochemistry, University of Bern, Freiestrasse 3, CH-3012 Bern 2, Switzerland

Received: February 23, 2010; Revised Manuscript Received: April 13, 2010

The development of functional materials based on the supramolecular organization of photoactive species in nanosized porous matrices requires a deep knowledge of host−guest interactions and of their influence on material properties and stability. Extensive first-principles investigations on the fluorescent dye fluorenone inside zeolite L, both at dry conditions and in the presence of water, have unraveled the molecular origin of the peculiar stability of this composite in humid environments, a fundamental prerequisite for practical applications. Results of first-principles molecular dynamics simulations, structural optimizations, and TDDFT calculations, validated by comparison with experimental data, provide a comprehensive picture of the structure, energetics, electronic excitation properties, and room-temperature behavior of the fluorenone/zeolite L composite and predict a substantial optical anisotropy for this material also maintained upon contact with water. The interaction of the fluorenone carbonyl group with the zeolite extraframework potassium cations is responsible for the dye stabilization in zeolite L nanochannels and features itself as a general leitmotiv regarding important properties of carbonyl functionalized photoactive species in hydrophilic matrices.

1. Introduction

Zeolites and mesoporous silica are successful host matrices for the supramolecular organization of a large variety of guests as well as key components of a novel promising class of hierarchically organized multifunctional hybrid materials.[1] The inclusion of photoactive molecules, complexes, or clusters into ordered one-dimensional channel systems is particularly intriguing, as the resulting host−guest compounds may exhibit peculiar properties, such as optical anisotropy, efficient energy transfer, nonlinear optical properties, enhanced stability, or specific photoactivity, thus opening the way for their exploitation in some of the most challenging fields of modern chemistry and material sciences. Novel perspectives have been disclosed by these materials in several research areas of interest, among which solar energy harvesting, processing/storing of information, and advanced sensing technology for analytics and diagnostics at the nanoscale are only some representative examples.[1−7] The zeolite-based materials are more advanced, with respect to organizational level and realization of practical applications, than materials based on mesoporous hosts.[1] Zeolite L (Figure 1) configures itself as an ideal host matrix because its arrays of parallel channels with small pore openings and cage diameters impose severe space restrictions and geometrical constraints to the guest species; as a result, very high concentrations of well-oriented photoactive molecules, which essentially behave as monomers, can be obtained. Considerable organization has been realized for organic dye−zeolite L composites, extending from the interior of a given crystal to the channel entrances and the external surface as well as from the microscopic to the macroscopic scale.[8] Diverse chemistry has been involved in the development of highly organized and functional host−guest materials, particularly also the design of molecules that are able to selectively adsorb at the channel entrances and establish communication between included guests and external objects.

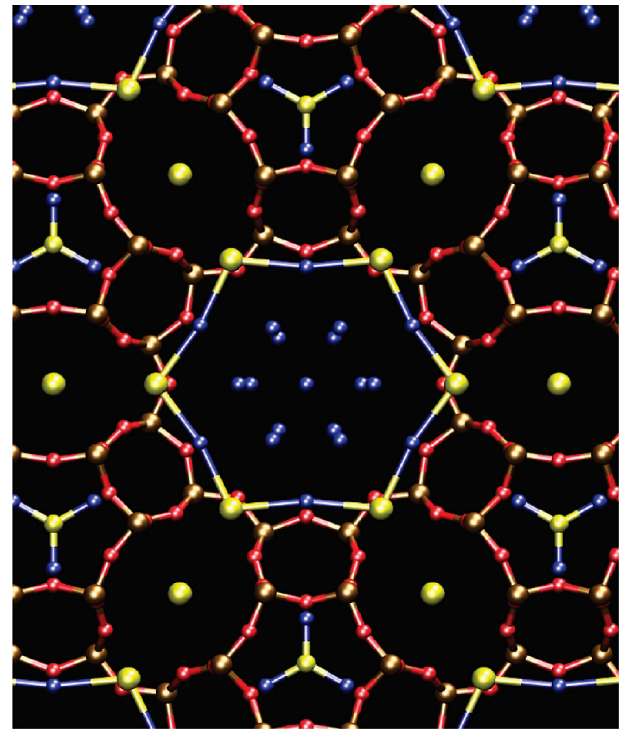

Figure 1. Ball-and-stick representation of perlialite ($K_{12}[Al_{12}Si_{24}O_{72}]\cdot 20H_2O$), the potassium-rich natural zeolite with an LTL framework topology, projected along the *c* axis, evidencing the location of the water sites in the 12-membered-ring channel. Color code: brown, T tetrahedral framework sites (Si or Al); red, framework O; yellow, K^+ sites; blue, water sites. Both K^+ and water sites have partial occupancy. The blue−yellow lines represent water−potassium coordination distances (2.77 Å).

* To whom correspondence should be addressed. Fax: (+) 39 031 2386630. E-mail: fois@fis.unico.it. URI: http://scienze-como.uninsubria.it/fois.

† University of Insubria.

‡ University of Bern.

10.1021/jp101635p
Published on Web 05/04/2010

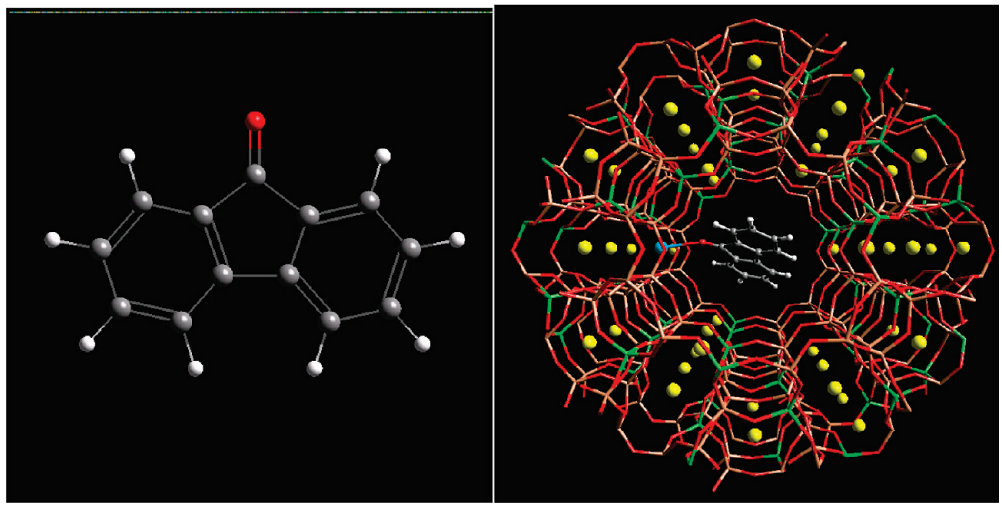

Figure 2. Left: ball-and-bonds representation of the fluorenone dye (gray, C; red, O; white, H). Right: representation of the fluorenone−zeolite L composite evidencing the one-dimensional channel system typical of the LTL framework. Color code: brown, Si; red, O; green, Al; gray, C; white, H; yellow, K; blue, potassium cation interacting with O_{Fl}.

The new guest−zeolite L-based building blocks are currently tested in devices. Because their size, morphology, composition, and optical properties need to be tailored to the specific task envisaged, the problems to be solved for realizing practical devices require efforts at the interface of chemistry, physics, and engineering. An atomistic level knowledge of intra- and intermolecular interactions inside the one-dimensional nanochannels of zeolite L would greatly help toward this aim. Clearly, the more sophisticated the new composites are, the more a detailed understanding is needed. Indeed, host−guest and guest−guest interactions not only may considerably influence the properties of the resulting material, leading, for example, to Davydov splitting,[9] as has been recently discussed,[8,10,11] but also determine, at a fundamental level, their stability, a basic condition for their practical application. In view of the well-known affinity of zeolites for water, stability of the hybrid material upon hydration is particularly critical and, unfortunately, many dye−zeolite composites do not meet this requirement. It was observed that, for example, exposure of dry *p*-terphenyl−zeolite L samples to air with a 22% relative humidity at room temperature leads to a displacement of the organic dye from the channels. Upon heating and hence drying, the molecule can be inserted again. Similar observations were also made for 1,6-diphenylhexatriene (DPH), for 1,2-bis-(5-methyl-benzoxazole-2-yl)ethane (MBOXE), and for other molecules of comparable structure.[12] In contrast to this, incorporated fluorenone[13] (Figure 2) is not displaced by water molecules under ambient conditions but remains inside the channels. This observation played an important role in the selection and hence realization of the first stopcock fluorophore-dye−zeolite L composites.[14] Detailed electronic absorption, fluorescence, infrared, and Raman spectroscopy as well as thermal analysis experiments have, therefore, been carried out in order to understand the interaction of the fluorenone with the host responsible of the resistance against substitution by water molecules. Such a feature was, however, not identified, and it was concluded that the fluorenone−zeolite L composite would make an excellent system for applying advanced theoretical calculations in order to improve our understanding of the host−guest interactions,[13] which is becoming a stringent necessity for designing and realizing more advanced host−guest composites with desired properties, functionality, and stability. Modeling studies aimed at investigating dye molecules' location inside zeolite cages have been performed in the past by means of molecular mechanics/force field techniques (see, for example, ref 15 and references therein). A sufficient level of accuracy and predictive power, as well as the possibility to perform optical property calculations, rely, however, on an explicit description of the electronic structure of the host−guest system, provided by quantum mechanical (first-principles) approaches.[16] Such kind of calculations, computationally more demanding, have become feasible for sufficiently large systems only very recently.[17] This allows us to report first-principles investigations on the interaction of the carbonyl fluorescent dye, fluorenone (Fl, $C_{13}H_8O$), with zeolite L (LTL) in its pure potassium form. Insight on the room-temperature behavior of the composite, both at dry conditions and in the presence of water, is gathered by first-principles molecular dynamics (FPMD),[18] which combines a density functional theory (DFT) level electronic structure treatment with a proper description of both periodic properties of crystalline structures and finite temperature effects. Such a technique has already contributed to revealing and rationalizing properties, behavior, and interactions of molecular systems confined in one-dimensional zeolitic channels.[17,19−22] In addition, a thorough characterization of structural properties and energetics of the dye−zeolite system is achieved through DFT-based optimizations, whereas time-dependent density functional theory (TDDFT)-calculated electronic absorption properties allow simulation results to be validated through comparison with experimental data.

On the whole, the present study provides for the first time a clear, reliable, and molecular-level picture of a photoactive host−guest composite at conditions close to those adopted in actual applications of zeolite-based functional materials, from which relevant features, otherwise difficult to access from experiments, emerged. The results presented in the following shed light on the dye positioning and orientational dynamics inside zeolite nanochannels and reveal their dependence on water content and indicate that fluorenone resistance against water substitution is due to the strong interaction of the dye carbonyl oxygen with the zeolite extraframework potassium cations, modulated by the collective properties of the water hydrogen-bonded network. Identification and understanding of such a stabilization mechanism, which could be generalized to other carbonyl containing dyes, paves the way to the realization of a

novel family of water-resistant composites featuring supramolecular organization of neutral luminescent molecules.

2. Experimental Section

Calculations on Fl/LTL systems were performed by adopting the PBE approximation[23] to density functional theory (DFT) and periodic boundary conditions. The simulation cell was twice the hexagonal experimental unit cell of the zeolite host along c ($a = b = 18.466$ Å; $c = 2 \times 7.476$ Å; $\beta = 120°$).[24] The framework content was $[T_{72}O_{144}]$, where T is a generic tetrahedral T site. Because, in LTL, there are two nonequivalent T sites, evenly and randomly occupied by Si and Al in a 3:1 ratio, the framework formula is $[Al_{18}Si_{54}O_{144}]$. With 18 monovalent extraframework cations to balance the framework negative charge, the simulation cell formula was $K_{18}[Al_{18}Si_{54}O_{144}]$ for the all-K form here considered,[24] in line with the composition of the LTL samples of ref 13. Only 8 out of 18 K^+ lie close to the walls of the 12-membered-ring channel and are, therefore, accessible to guest molecules, while the remaining ones are caged in the smaller cancrinite and ε cages. Three dye−zeolite model systems were investigated: dry Fl/LTL ($K_{18}[Al_{18}Si_{54}O_{144}]$Fl), built by inserting one Fl molecule in the computational supercell (see Figure 2 for a graphical representation), and two hydrated systems $K_{18}[Al_{18}Si_{54}O_{144}]Fl\cdot(H_2O)_n$, with $n = 4$ (4W) and $n = 8$ (8W), modeling low- and high-water loading conditions, respectively. The systems are, therefore, characterized by a concentration of 0.5 Fl molecules per unit cell, whereas experimental data on Fl/LTL refer to a composite with 0.2 dye molecules per cell.[13] Besides these systems, mono- and dihydrated LTL models ($K_{18}[Al_{18}Si_{54}O_{144}]\cdot(H_2O)_n$, $n = 1, 2$) were considered and their geometry optimized by using the same computational protocol adopted for the dye-containing systems.

Electron−ion core interactions were calculated with ultrasoft Vanderbilt pseudopotentials for H, C, and O and norm conserving pseudopotentials for Si, Al, and K (semicore).[25] Electronic orbitals were expanded in planewaves up to a 25 Ry cutoff (200 Ry for the density). This electronic structure calculation scheme provided a proper description of large host−guest systems.[22,26]

FPMD[18] studies were performed on the three dye−zeolite models Fl/LTL, 4W, and 8W by adopting a time step of 0.121 fs and an inertia parameter of 500 au for the electronic state coefficients. After equilibration, trajectories ∼10 ps long were collected and analyzed. Simulations were performed in the microcanonical ensemble (average temperature = 300 K). Local energy minima were obtained by geometry optimization of selected configurations extracted from the simulations (convergence criterion = 5×10^{-4} au for atom forces). Binding energies for the Fl/K^+ and H_2O/K^+ pairs both in the gas phase and in LTL were calculated by using the same scheme for the electronic structure treatment (see the Supporting Information for tests at higher levels of theory on related gas-phase systems).

Electronic excitations[27] were calculated with the time dependent DFT (TDDFT) and a Gaussian basis set[28] on B3LYP[29] densities for selected molecular models (clusters) cut from the optimized periodic systems (see Figure 4 and the Supporting Information for graphical representations of the clusters). The 6-311++G(d,p) and the 6-31+G(d) basis sets were used for the Fl atoms and for framework oxygens, respectively, with ECP pseudopotentials and corresponding basis sets for K, Al, and Si.[30] In the water-containing cluster models, 6-31+G(d) and 3-21+G(d) basis sets were adopted for the O and H atoms of water, respectively. Clusters were capped with H atoms by replacing outermost Si−O−Si bridges with Si−O−H and fixing the OH distance to 1.0 Å. Such a procedure for extracting clusters from periodic systems has been tested and successfully adopted in the past.[22,31]

3. Results

3.1. The Dry Fl/LTL System. The dry Fl/LTL model system was set up by positioning Fl close to the center of the LTL channel, and its behavior at room-temperature conditions was followed by FPMD. In the first phases of the dry Fl/LTL system simulation, the dye molecule, in search for its optimal positioning, explored a broad range of different orientations but preferentially sampled those where its carbonyl oxygen was directed toward the channel walls, where accessible K^+ ions are located (see the movie in the Supporting Information). Drastic reorientations were no longer observed after equilibration: the molecule only oscillated around the channel axis so as to switch its carbonyl oxygen O_{Fl} from a K^+ ion (K_1) to a neighboring one (K_2; see the labels in Figure 3). The time evolution of the Fl/LTL system evidenced three types of frequently visited configurations: (i) O_{Fl} interacting with K_1, (ii) O_{Fl} interacting with K_2, and (iii) O_{Fl} midway between K_1 and K_2. Geometry optimizations were performed on a representative set of configurations, characterized by different Fl orientations, sampled from the trajectory.

A selection of the resulting structures is shown in Figure 3. In the minimum energy structure OPT_a, fluorenone is strongly bound to one K^+ (K_1): O_{Fl} is 2.59 Å from K_1, and the C−O_{Fl} bond is significantly longer than in the gas-phase (Table 1). In OPT_b, only 2.1 kcal/mol higher in energy, the dye is involved in two contacts with K_1 and K_2, located at 2.79 and 2.93 Å from O_{Fl}, respectively, and its carbonyl bond is elongated as in OPT_a. On the other hand, the OPT_c geometry is 30.8 kcal/mol less stable than the minimum. In this structure,[32] the Fl carbonyl group points toward an AlO_4 tetrahedron, the C−O_{Fl} distance is close to the gas-phase value, and O_{Fl} is well separated from the extraframework cations ($d(K^+-O_{Fl}) \sim 5$ Å). Thus, while arrangements dominated by Fl−K^+ interactions have comparable stability, Fl orientations where O_{Fl} is not in close contact with K^+ are energetically disfavored.

UV/vis spectra of Fl/LTL samples (measured in the presence of air)[13] show features and an intensity distribution similar to those exhibited by Fl in nonpolar media solutions (such as, for example, cyclohexane, (CH)); they are, however, broader and red shifted. In particular, the longest-wavelength band due to the Fl $1\pi \rightarrow 1\pi^*$ (HOMO−LUMO) transition undergoes a ∼50 nm bathochromic shift in passing from $\sim 10^{-5}$ M cyclohexane solutions to the zeolite environment.[13] The excitation spectrum calculated for the Fl/LTL structure OPT_a is compared to those of Fl in the gas phase and in CH in Figure 4 (see Table 1 for excitation wavelengths and assignments). Calculated absorption features are in good agreement with experiments.[13,33] The Fl $1\pi \rightarrow 1\pi^*$ excitation, 402 nm in the gas phase, is found at 415 nm in CH and at 456 nm in OPT_a. A greater red shift, to 470 nm, is obtained for the other favorable Fl orientation OPT_b, where O_{Fl} is close to two K^+ ions, thus rationalizing also the observed broadening of the spectral features.[13] On the other hand, the $1\pi \rightarrow 1\pi^*$ excitation is blue shifted to 390 nm in OPT_c; that is, spectra of model structures with no $O_{Fl}-K^+$ close contacts do not correlate with experiment. To establish whether the observed red shift is caused directly by the $O_{Fl}-K^+$ interaction or, indirectly, by K^+-induced distortions of the Fl geometry (for example, the C═O bond elongation), electronic excitations were calculated on the dye molecule extracted from the OPT_a structure (Fl OPT_a). The resulting spectrum (Figure 4) is very close to that obtained for the dye in cyclohexane.

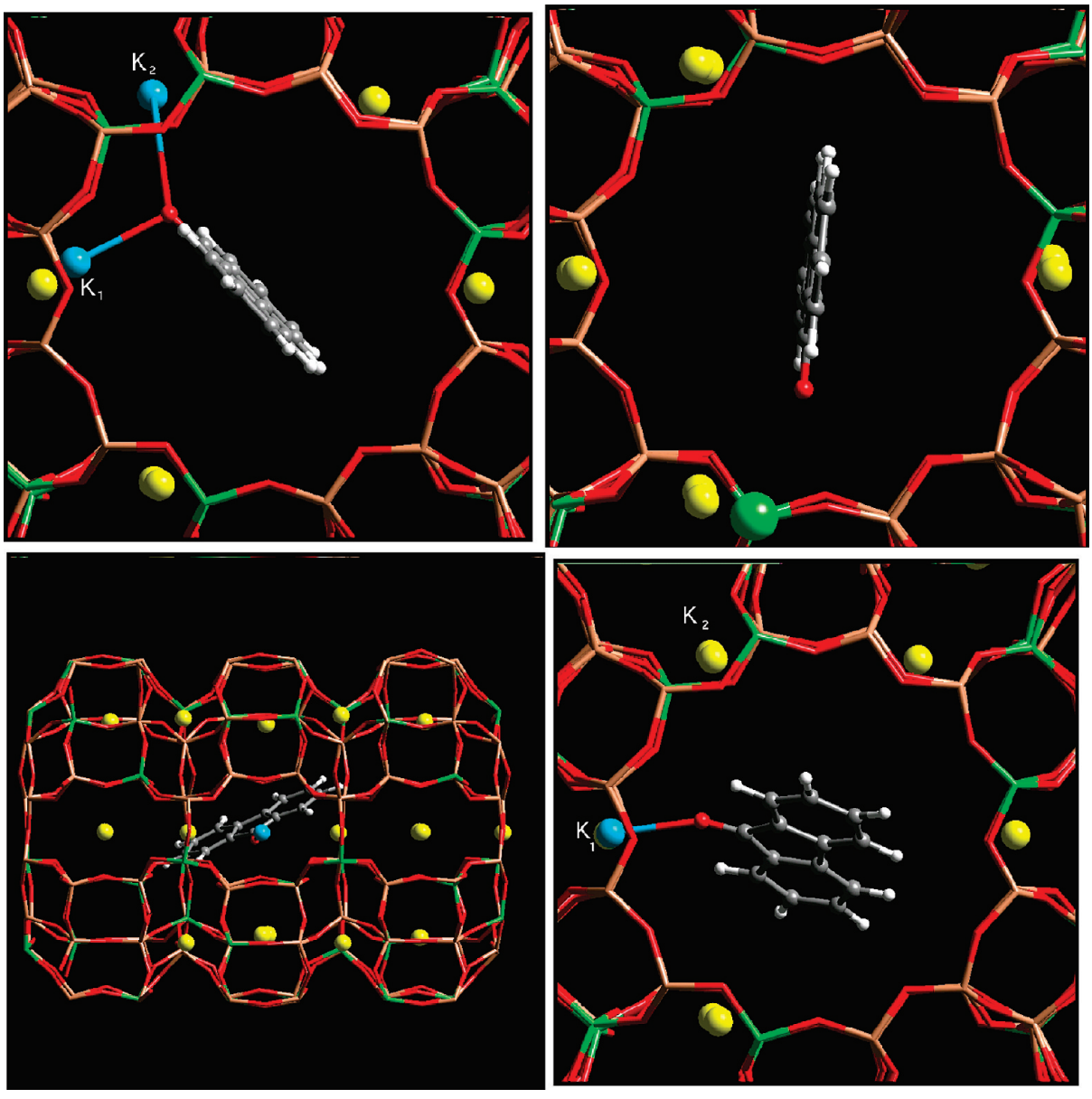

Figure 3. Bottom panels: representations of the minimum energy structure OPT_a of the dry Fl/LTL system in the LTL channel section (left) and along the channel axis (right) (brown, Si; red, O; green, Al; gray, C; white, H; yellow, K; blue, cation interacting with O_{Fl} (K_1)). Top left: structure of OPT_b (blue, K_1 and K_2). Top right: structure of OPT_c. The green sphere indicates the Al atom closest to O_{Fl}.

TABLE 1: Electronic Excitation Energies (nm), HOMO and LUMO Orbital Energies (eV), and C=O Bond Length (Å) of Fl in Selected Optimized Structures

systems[a]	Fl/gas	Fl/CH[b]	Fl OPT_a	OPT_a[c]	OPT_b[c]	$8W_a$[c]	$8W_b$[c]
$1\pi \rightarrow 1\pi^*$	401.7	415.3	414.8	456.1	469.8	445.9	459.1
$2\pi \rightarrow 1\pi^*$	310.3	316.0	316.9	335.4	339.5	329.5	337.6
$3\pi \rightarrow 1\pi^*$	279.4	285.5	285.3	293.0	294.2	290.7	294.0
$1\pi \rightarrow 2\pi^*$	253.6	256.5	255.9	257.9	255.8	259.7	257.6
$4\pi \rightarrow 1\pi^*$	244.8	248.6	249.9	260.3	262.3	257.0	262.0
E_{homo}	−6.586	−6.656	−6.600	−6.673	−7.001	−9.635	−9.449
E_{lumo}	−2.695	−2.863	−2.803	−3.133	−3.534	−6.073	−5.932
d (C=O)	1.220	1.231	1.246	1.246	1.246	1.246	1.247

[a] From left to right: gas-phase FL (Fl/gas), Fl in cyclohexane (Fl/CH), Fl molecule extracted from OPT_a (Fl OPT_a), dry Fl−zeolite L systems (OPT_a and OPT_b), and highly hydrated Fl−zeolite L systems ($8W_a$, $8W_b$). All geometries optimized at the DFT (PBE) level (tests with other levels of theory in the Supporting Information). [b] CH solvent molecules explicitly modeled (see the Supporting Information). [c] TDDFT excitation energies and orbital energies refer to clusters derived from periodic DFT optimized structures and are calculated at the B3LYP level.

Finally, in both OPT_a and OPT_b structures, the energy lowering with respect to the gas phase calculated for the $1\pi^*$ state is larger than that obtained for 1π (Table 1). On this basis, it can be concluded that the bathochromic shift experimentally detected in Fl/LTL spectra is due to close contacts between the dye carbonyl group and the extraframework cations, which primarily stabilize the Fl levels localized on the carbonyl oxygen and, in particular, the $1\pi^*$ state (the Fl LUMO; see Figure 4).[34]

3.2. Hydrated Systems. Upon hydration, water molecules, in principle, could be in competition with Fl for coordinating the potassium cations, thus displacing the dye from its anchoring place. To quantify such a competitive effect, the $Fl-K^+$ and H_2O-K^+ binding energies were calculated both in the gas phase and in the zeolite environment. In the latter case, the energy minimum of the dry dye/zeolite composite OPT_a was compared with the optimized geometry of a model monohydrated LTL system (LTL/W), represented in Figure 5, where water was found to be ligated to the same potassium cation K_1 that coordinated Fl in OPT_a. The $Fl-K^+$ interaction is stronger than

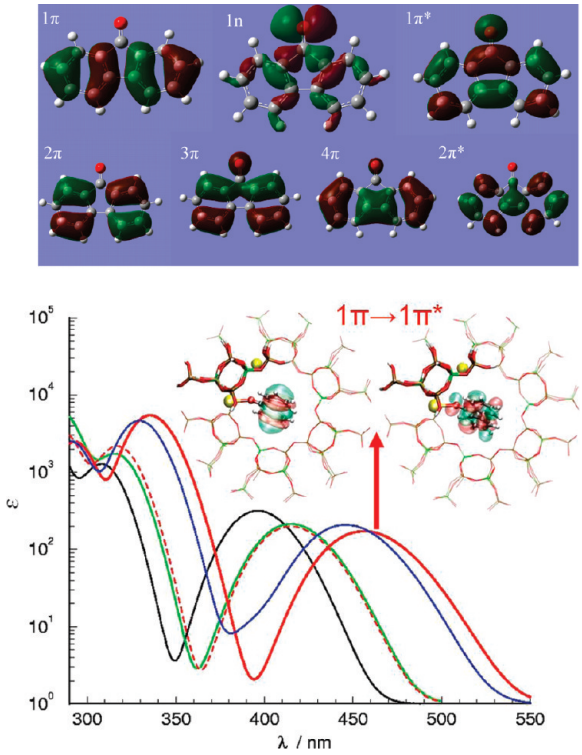

Figure 4. TDDFT electronic excitation spectra calculated for gas-phase Fl (black), Fl in cyclohexane (green), Fl/LTL energy minimum OPT_a (red), Fl extracted from OPT_a (red dashed), and $8W_a$ energy minimum (blue). The top inset shows the frontier molecular orbitals of gas-phase Fl involved in the transitions (no significant mixing of these orbitals with zeolite states occurs in the Fl/LTL models). The central inset shows the HOMO and LUMO obtained for the cluster cut from OPT_a used for the TDDFT calculation (cluster atoms = thicker lines). Atom color code: brown, Si; red, O; green, Al; gray, C; white, H; yellow, K.

the H_2O-K^+ one, both in the gas phase (28.2 vs 17.4 kcal/mol) and in LTL (19.3 vs 11.6 kcal/mol, respectively). Fl might interact with K^+ also through its C=C bonds according to a cation−π-bond interaction; indeed, the gas-phase binding energy calculated for a Fl/K^+ π complex is significant, 15.8 kcal/mol, but lower than that associated with the structure with a $O_{Fl}-K^+$ contact. Therefore, at a very low water content (one H_2O per Fl), Fl is not displaced from zeolite L because the $O_{Fl}-K^+$ interaction is dominant. Because, at higher water loadings, cooperative hydrogen bond effects can influence significantly both interactions and behavior inside zeolite nanochannels,[17,20,35−37] LTL models containing two water molecules were investigated as well: one with the molecules positioned in adjacent unit cells, thus well separated from each other (LTL/2W), and the second one with a water dimer (LTL/W_2). The resulting optimized structures are represented in Figure 5, whereas calculated binding energies are reported in Table 2.

In the LTL/2W system, the binding energy per H_2O molecule is slightly lower with respect to the monohydrated system; on the other hand, an increase of the binding energy per molecule is observed in LTL/W_2. The LTL/2W system features two independent water molecules and is, therefore, quite similar to LTL/W: in both cases, water is coordinated to K^+ with its oxygen atom at a distance of ~2.7 Å from the cation, and the protons are directed toward the center of the channel. The picture drastically changes in passing to the LTL/W_2 system, characterized by the presence of a water dimer. Here, one of the water molecules interacts with two potassium cations (K_1 and K_2) through its oxygen atom, while its protons are involved in two strong hydrogen bonds with a framework oxygen and with the other water molecule, respectively. It should be pointed out that such a water arrangement is strongly reminiscent of that determined by a diffraction study in the hydrated potassium-rich form of natural zeolite L (perlialite),[38] where the water sites close to the LTL channel walls are located between two neighboring K^+ sites (see Figure 1). In line with the above considerations, even though the structure with two independent water molecules is characterized by stronger $K-O_w$ interactions, the LTL system containing the water dimer ligated to two K^+ was found to be energetically favored (by 6 kcal/mol). These findings indicate that Fl binding is still favored with respect to water at a 2:1 H_2O-to-Fl ratio (see Table 2) and highlight the relevance of water hydrogen bond effects in LTL, which suggested a thorough investigation of the dye−zeolite composite at higher water loadings. To this aim, the room-temperature behavior of hydrated LTL models containing Fl and four or eight water molecules per Fl (4W and 8W, respectively) was simulated.

When four H_2O per Fl are present, the encapsulated dye molecule behaves as in dry conditions, with its O_{Fl} preferentially ligated to K_1 and, occasionally, to K_2. Such interactions are not perturbed by water molecules, which do not bind to O_{Fl} and are coordinated to different K^+. On the other hand, water forms hydrogen bonds with O_{Fl} and competes with the dye in binding to the same K^+ in the 8W system (eight H_2O per Fl), where the water content is high enough to allow, in principle, each accessible potassium cation to be coordinated by at least one H_2O molecule. However, during the 8W simulation, the dye molecule, instead of being displaced by water, remains preferentially oriented as in dry conditions, that is, with its carbonyl oxygen pointed toward K_1 and/or K_2 (see the movie in the Supporting Information).

Hydration effects in the 4W and 8W systems may be quantitatively evaluated by inspecting the distributions of relevant interatomic distances (rdf), reported in Figure 6. A peak at 1.85 Å appears in the O_{Fl}−water proton rdf ($H-O_{Fl}$) of the 8W system, indicating that, by increasing the water loading, O_{Fl} becomes involved in hydrogen bonds with H_2O molecules. Concomitantly, the O_{Fl}−potassium ($K-O_{Fl}$) rdf peak, at 2.70 Å for both dry and 4W systems, becomes broader and displaced toward larger distances (2.90 Å). Therefore, $O_{Fl}-K^+$ interactions, although weaker, still persist at high hydration. Interestingly, in doubling the H_2O/Fl ratio, both water−water and water−framework oxygen distances decrease, while the K^+−water separation increases (from 2.79 to 2.86 Å). This finding indicates that, as already suggested by the relative stabilities of the dihydrated LTL systems, the increase of water loading in LTL leads to an enhancement of hydrogen bond interactions. Moreover, in 8W, a K^+ ion leaves its site close to the walls and becomes engaged in a π interaction with one of the Fl C_6 rings. Framework oxygens and H_2O molecules complete the coordination of this cation (see Figure 7 and the movie in the Supporting Information).

As for the dry system, different energy minima have been obtained for the 8W model by optimizing selected configurations sampled along the trajectory. The two lowest minima, represented in Figure 7, clearly show that, despite water competitive effects in binding, the dye interaction with K^+ is maintained. In particular, in one of the structures ($8W_a$), O_{Fl} is coordinated to K_1 and K_2, which are also ligated to one water molecule each, whereas in $8W_b$, O_{Fl} coordinates only K_1 but is involved in a hydrogen bond with a water molecule as well. The two structures, characterized by different $O_{Fl}-K$ binding, water−

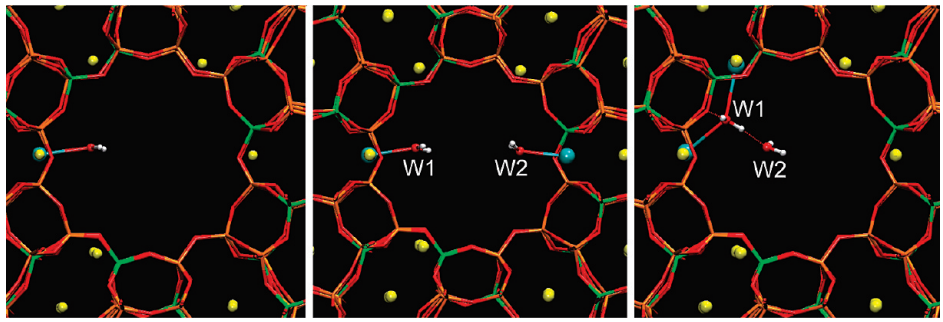

Figure 5. Representations of the optimized structures of the monohydrated system LTL/W (left) and of the dihydrated systems LTL/2W (center) and LTL/W_2 (right). (brown, Si; red, O; green, Al; gray, C; white, H; yellow, K; cyan, K cations interacting with water oxygens (O_w)).

TABLE 2: Binding Energies (BEs) (kcal/mol) and Relevant Interatomic Separations (Å) for the Gas-Phase Systems Fl−K^+ and H_2O−K^+ and for the Zeolite Models Fl/LTL, LTL/W, LTL/2W, and LTL/W_2

systems	binding energy	oxygen−potassium distances	carbonyl bond distances	hydrogen bond distances
K^+−Fl	28.2	$r(K^+-O_{Fl})$ 2.454	$r(C-O_{Fl})$ 1.251	
K^+−H_2O	17.4	$r(K^+-O_w)$ 2.628		
Fl/LTL	19.3	$r(K_1-O_{Fl})$ 2.590	$r(C-O_{Fl})$ 1.246	
LTL/W	11.6	$r(K_1-O_w)$ 2.768		
LTL/2W	10.4[a]	$r(K_1-O_{w1})$ 2.737		
	9.3[b]	$r(K_3-O_{w2})$ 2.710		
LTL/W_2[c]	13.5[a]	$r(K_1-O_{w1})$ 2.854		$r(H^1_{w1}-O)$ 1.904
	15.3[b]	$r(K_2-O_{w1})$ 3.009		$r(H^2_{w1}-O_{w2})$ 1.890

[a] Binding energies per water molecule: BE = $-[E(LTL\cdot 2H_2O) - E(LTL) - 2 \times E(H_2O)]/2$. [b] Incremental binding energy: BE = $-[E(LTL\cdot 2H_2O) - E(LTL/W) - E(H_2O)]$. [c] The energy difference $E(LTL/2W) - E(LTL/W_2)$ amounts to 6.0 kcal/mol.

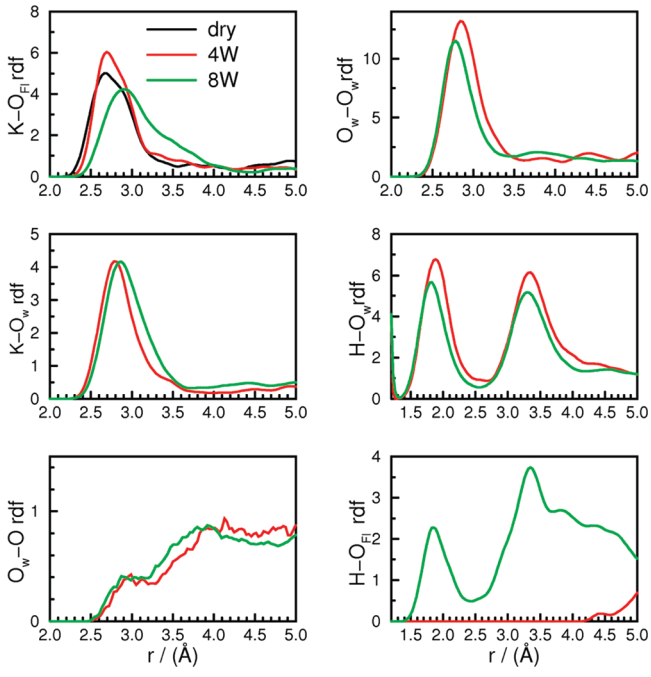

Figure 6. Radial distribution functions (rdf) calculated for dry Fl/LTL (black), low water loading 4W (red), and high water loading 8W (green). Abbreviations: O_w, water oxygens; H, water hydrogens; O, framework oxygens.

potassium coordination, and hydrogen-bonding arrangements of the water molecules, are almost isoenergetic ($\Delta E(8W_a - 8W_b) = -0.8$ kcal/mol). The electronic absorption spectrum calculated for the $8W_a$ structure is reported in Figure 4. Because of the larger K^+−O_{Fl} separation with respect to dry Fl/LTL (3.041 and 3.002 Å from K_1 and K_2, respectively), the stabilizing effect of the extraframework cation on the Fl LUMO is less pronounced than in the absence of water. As a result, the calculated red shift of the Fl $1\pi \rightarrow 1\pi^*$ band (found at 446 nm) with respect to the spectrum in CH is smaller (~30 vs ~40 nm).

On the other hand, in $8W_b$, a $1\pi \rightarrow 1\pi^*$ peak at longer wavelengths is obtained because the potassium cation is closer to O_{Fl} than in $8W_a$, thus resulting in a greater stabilization of the Fl LUMO (Table 1). A water proton, at a hydrogen bond distance (2.006 Å) from O_{Fl}, also contributes to $1\pi^*$ stabilization.

On the whole, both room-temperature behavior and energy minima of the highly hydrated composite indicate that, in wet conditions, not only Fl keeps contact with K^+ but also its average position and orientation inside the channel show only modest changes. Further insight on the dye orientation can be obtained from the distributions of the angle α of the Fl electronic transition moment with the channel axis, $d(\alpha)$, along the FPMD trajectories. The calculated distributions, shown in Figure 8, indicate anisotropy for the dye−zeolite composite independent of the water content. In particular, the position of the maximum is slightly shifted to lower angles with increasing hydration (24, 21, and 18° for dry Fl/LTL, 4W, and 8W, respectively). Interestingly, in 8W, $d(\alpha)$ becomes neatly bimodal, suggesting that the high-water loading regime modifies the dynamical behavior of the encapsulated dye. Indeed, the Fl orientational lifetime is roughly twice than in dry and low-water loading conditions, as indicated by the α time autocorrelation functions $\langle\alpha(t)\alpha(0)\rangle$ (Figure 8). This finding can be rationalized by considering that, in the 8W system, Fl is involved in the water hydrogen bond network: its reorientation is, therefore, hampered by the energetic cost of the hydrogen bond rearrangements.

4. Discussion

The room-temperature behavior and the energetic, as well as the structural and electronic, properties of the Fl/LTL models considered herein reveal a key role of the interactions between the fluorenone carbonyl oxygen and K^+ cations in the dye−zeolite composite, which supports, complements, and rationalizes experimental findings. As indicated by the greater binding energy of the dye−zeolite adduct (19.3 kcal/mol) relative to H_2O−LTL (11.6 kcal/mol), the strong $K^+\cdots O{=}C$ interaction explains, for example, why the evacuation temperature of fluorenone from LTL (≥773 K) is much higher than that of water (373 K).[13] In light of the present results, the fact that such a high temperature, well above the fluorenone sublimation point (543 K),[13] is needed to evacuate Fl from zeolite L channels, is particularly noteworthy. Indeed, besides being a manifestation of the composite stability, it highlights the relevance of the extraframework K^+ cations in stabilizing carbonyl-functionalized guest species inside zeolitic nanochannels.[39]

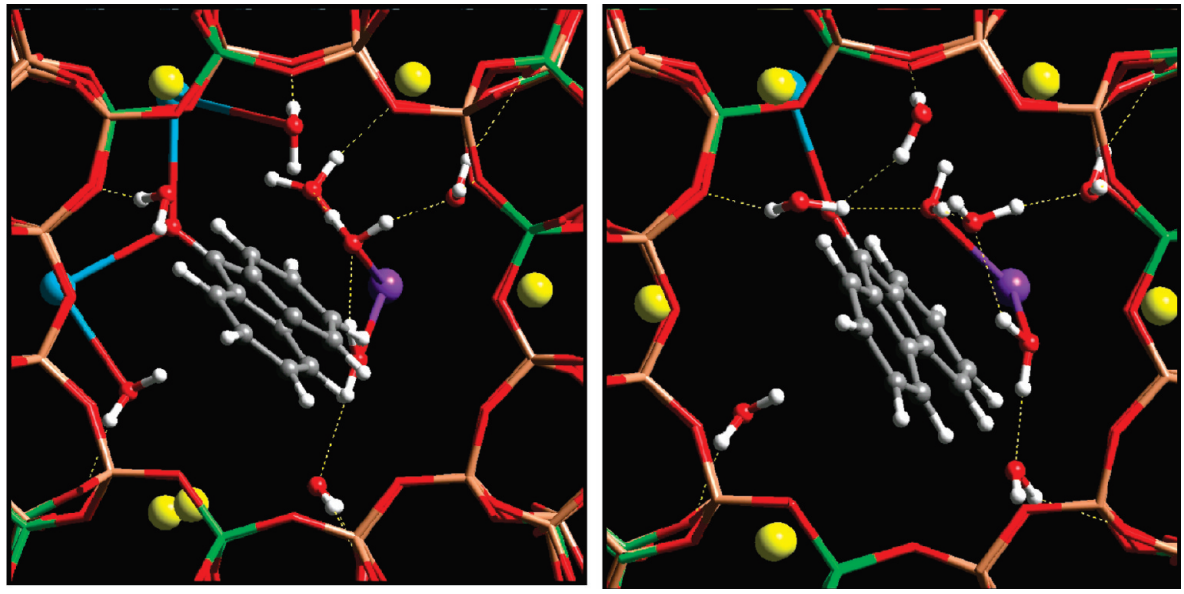

Figure 7. Graphical representation of the optimized structures $8W_a$ (left) and $8W_b$ (right) for the 8W system. Color code: brown, Si; red, O; green, Al; gray, C; white, H; yellow, K^+; blue, K_1 and K_2 ($8W_a$) and K_2 ($8W_b$); violet, K^+ π-bonded to Fl; yellow dotted lines, hydrogen bonds.

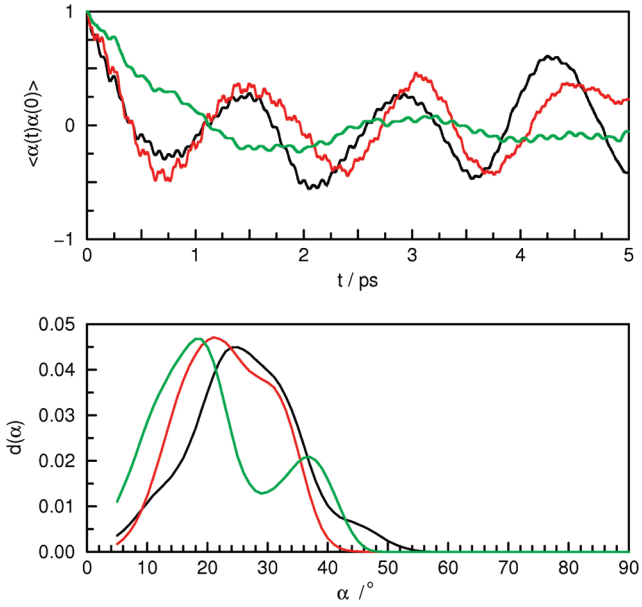

Figure 8. Bottom panel: distribution of the angle α formed by the electronic transition moment (parallel to the long molecular axis) and the LTL channel axis. Top panel: normalized orientational time autocorrelation function $<\alpha(t)\alpha(0)>$. Color code: black, dry Fl/LTL; red, 4W; green, 8W.

As demonstrated here, on the basis of TDDFT calculations, the experimentally detected red shift in the UV/vis spectra of the Fl/LTL composite with respect to fluorenone in the gas phase and in apolar solvents is a signature of the $K^+\cdots O{=}C$ interaction, which stabilizes the fluorenone LUMO level, thus lowering the HOMO−LUMO energy gap. In perspective, such a finding, together with the thorough understanding of the zeolite environment's effects on the Fl electronic structure gathered herein, will be of help in future work aimed at the characterization of the luminescence properties and excited-state dynamics of the composite.[21]

A further relevant issue investigated in the present study is the orientation of the caged dye. The location and orientation of molecular species inside the channels depend on a broad variety of factors, such as size, shape, and charge of the guest, besides on preparation conditions, and are, therefore, difficult to predict or to gather from experiment. Specifically, the orientation of the dye molecule can be directly deduced from optical data only in few cases. The simulation study presented here, validated by the favorable comparison with experimental data, has provided valuable insight into this aspect as well. In particular, calculations predict substantial anisotropy of the Fl/zeolite L composite independent of the degree of hydration of LTL nanochannels. Moreover, water coadsorption induces a remarkable slowdown of the dynamical properties of the dye molecule, which can be understood on the basis of water collective properties.

Water effects, negligible at low loadings, become relevant when its content is high enough to allow formation of a hydrogen-bonded network inside the LTL channels, which involves zeolite framework oxygens and incorporates extraframework cations and the dye molecule. At these conditions, the collective properties of water molecules are dominated by hydrogen bonding, in line with previous work on zeolitic water.[20,40] An increase in the number and strength of hydrogen bonds implies a frictioning of the water orientational motion in zeolite nanochannels due to the energy cost of water connectivity changes; the dye reorientation is slowed down as well because its carbonyl group takes part in the hydrogen-bonding network. Water alters the Fl dynamical behavior but does not affect significantly the dye excitations: indeed, on comparison of the spectra calculated for the minimum energy structures of the dry and highly hydrated model composites, only a small blue shift with respect to dry conditions is detected. The molecular origin of this effect is that water coabsorption induces a modest increase of the average $O_{Fl}-K^+$ separation, which implies a lower stabilization of the dye LUMO, principally localized on its carbonyl oxygen. These results indicate that the composite optical properties are maintained in the presence of water, a fundamental prerequisite in the perspective of practical applications in humid environments.

5. Conclusions

The computational results herein presented provide an atomistic level rationale for the stability of the fluorenone dye−zeolite L composite in the presence of water. The

interaction of the fluorenone carbonyl group with the zeolite extraframework potassium cations has been identified as the leitmotiv of both the stability of the dye−zeolite composite and the anisotropy of such a fluorescent dye in the nanochannels of zeolite L. Water molecules do not displace fluorenone from zeolite L because the $K^+\cdots O{=}C$ interaction is dominant; rather, they share the channel space with the dye and finely tune its observable electronic and optical properties through hydrogen bond interactions.

Such an issue, which could be generalized to other carbonyl-functionalized dyes, represents a step forward toward the design, based on the knowledge of the host−guest interactions, of dye−zeolite composites with ordered supramolecular arrangements as building blocks for the fabrication of optical devices operating in diverse conditions.

Acknowledgment. On the occasion of his retirement, we dedicate this paper to Prof. Dr. Aldo Gamba. This work was supported by MIUR (PRIN2007 and PRIN2006).

Supporting Information Available: Full citation of ref 27, additional computational details and results (Tables S1−S5, Figures S1−S6), movie of the dry Fl/LTL system, and movie of the highly hydrated 8W fluorenone−zeolite composite. This material is available free of charge via the Internet at http://pubs.acs.org.

References and Notes

(1) (a) Brühwiler, D.; Calzaferri, G.; Torres, T.; Ramm, J. H.; Gartmann, N.; Dieu, L. Q.; López-Duarte, I.; Martínez Díaz, M. *J. Mater. Chem.* **2009**, *19*, 8040–8067. (b) Wang, Y.; Li, H.; Feng, Y.; Zhang, H.; Calzaferri, G.; Ren, T. *Angew. Chem., Int. Ed.* **2010**, *49*, 1434–1438.

(2) (a) Calzaferri, G.; Huber, S.; Maas, H.; Minkowski, C. *Angew. Chem., Int. Ed.* **2003**, *42*, 3732–3758. (b) Hashimoto, S.; Samata, K.; Shoji, T.; Taira, N.; Tomita, T.; Matsuo, S. *Microporous Mesoporous Mater.* **2009**, *117*, 220–227. (c) Lee, J. S.; Ha, K.; Lee, Y. J.; Yoon, K. B. *Top. Catal.* **2009**, *52*, 119–139. (d) Li, H. R.; Cheng, W. J.; Wang, Y.; Liu, B. Y.; Zhang, W. J.; Zhang, H. J. *Chem.−Eur. J.* **2010**, *16*, 2125–2130. (e) Tsotsalas, M.; Kopka, K.; Luppi, G.; Wagner, S.; Law, M. P.; Schäfers, M.; De Cola, L. *ACS Nano* **2010**, *4*, 342–348. (f) Vohra, V.; Calzaferri, G.; Destri, S.; Pasini, M.; Porzio, W.; Botta, C. *ACS Nano* **2010**, *4*, 1409–1416.

(3) Kim, H. S.; Pham, T. T.; Yoon, K. B. *J. Am. Chem. Soc.* **2008**, *130*, 2134–2135.

(4) (a) Shim, T.; Lee, M. H.; Kim, D.; Kim, H. S.; Yoon, K. B. *J. Phys. Chem. B* **2009**, *113*, 966–969. (b) van der Veen, M. A.; Valev, V. K.; Verbiest, T.; De Vos, D. E. *Langmuir* **2009**, *25*, 4256–4261. (c) Ramamurthy, V. In *Photochemistry in Organized and Constrained Media*; Ramamurthy, V., Ed.; VCH Publishers: New York, 1991; pp 429−493.

(5) Inagaki, S.; Othani, O.; Goto, Y.; Okamoto, K.; Ikai, M.; Yamanaka, K.; Tani, T.; Okada, T. *Angew. Chem., Int. Ed.* **2009**, *48*, 4042–4046.

(6) Valtchev, V.; Mintova, S.; Tsapatsis, M. *Ordered Porous Solids, Recent Advances and Prospects*; Elsevier: Amsterdam, The Netherlands, 2009.

(7) Corma, A.; García, H. *Eur. J. Inorg. Chem.* **2004**, 1143–1164.

(8) Calzaferri, G.; Lutkouskaya, K. *Photochem. Photobiol. Sci.* **2008**, *7*, 879–910.

(9) Davydov, A. S. *Usp. Fiz. Nauk.* **1964**, *82*, 393–448.

(10) Busby, M.; Blum, C.; Tibben, M.; Fibikar, S.; Calzaferri, G.; Subramaniam, V.; De Cola, L. *J. Am. Chem. Soc.* **2008**, *130*, 10970–10976.

(11) Calzaferri, G. *Nuovo Cimento* **2008**, *123 B*, 1337–1367.

(12) Pauchard, M.; Devaux, A.; Calzaferri, G. *Chem.−Eur. J.* **2000**, *6*, 3456–3470.

(13) Devaux, A.; Minkowski, C.; Calzaferri, G. *Chem.−Eur. J.* **2004**, *10*, 2391–2408.

(14) Maas, H.; Calzaferri, G. *Angew. Chem., Int. Ed.* **2002**, *41*, 2284–2288.

(15) Fuchs, A. H.; Cheetham, A. K. *J. Phys. Chem. B* **2001**, *105*, 7375–7383.

(16) Bussemer, B.; Munsel, D.; Wünscher, H.; Mohr, G. J.; Grummt, U.-W. *J. Phys. Chem. B* **2007**, *111*, 8–15.

(17) Tabacchi, G.; Gamba, A.; Fois, E. Intracage Chemistry in Zeolitic Systems: The Car-Parrinello Approach. In *Quantum Chemical Calculations of Surfaces and Interfaces of Materials*; Basiuk, V. A., Ugliengo, P., Eds.; American Scientific Publishers: Stevenson Ranch, CA, 2009; pp 65−87.

(18) (a) Car, R.; Parrinello, M. *Phys. Rev. Lett.* **1985**, *55*, 2471–2475. (b) Marx, D.; Hutter, J. *Ab Initio Molecular Dynamics*; Cambridge University Press: Cambridge, U.K., 2009. (c) *CPMD Code*; MPI für Festkörperforschung: Stuttgart, Germany, IBM Zürich Research Laboratory: Zürich, Switzerland, 1990−2009; www.cpmd.org.

(19) (a) Fois, E.; Tabacchi, G.; Quartieri, S.; Vezzalini, G. *J. Chem. Phys.* **1999**, *111*, 355–359. (b) Quartieri, S.; Sani, A.; Vezzalini, G.; Galli, E.; Fois, E.; Gamba, A.; Tabacchi, G. *Microporous Mesoporous Mater.* **1999**, *30*, 77–87. (c) Fois, E.; Gamba, A.; Tabacchi, G.; Ferro, O.; Quartieri, S.; Vezzalini, G. *Stud. Surf. Sci. Catal.* **2002**, *142*, 1877–1884. (d) Ferro, O.; Quartieri, S.; Vezzalini, G.; Fois, E.; Gamba, A.; Tabacchi, G. *Am. Mineral.* **2002**, *87*, 1415–1425. (e) Fois, E.; Gamba, A.; Medici, C.; Tabacchi, G.; Quartieri, S.; Mazzuccato, E.; Arletti, R.; Vezzalini, G.; Dmitriev, V. *Microporous Mesoporous Mater.* **2008**, *115*, 267–280.

(20) (a) Fois, E.; Gamba, A.; Tabacchi, G.; Quartieri, S.; Vezzalini, G. *J. Phys. Chem. B* **2001**, *105*, 3012–3016. (b) Fois, E.; Gamba, A.; Tabacchi, G.; Quartieri, S.; Vezzalini, G. *Phys. Chem. Chem. Phys.* **2001**, *3*, 4158–4163.

(21) Fois, E.; Gamba, A.; Medici, C.; Tabacchi, G. *ChemPhysChem* **2005**, *6*, 1917–1922.

(22) Tilocca, A.; Fois, E. *J. Phys. Chem. C* **2009**, *113*, 8683–8687.

(23) Perdew, J. P.; Burke, K.; Ernzerhof, M. *Phys. Rev. Lett.* **1996**, *77*, 3865–3868.

(24) Newsam, J. M. *J. Phys. Chem.* **1989**, *93*, 7689–7694.

(25) (a) Vanderbilt, D. *Phys. Rev. B* **1990**, *41*, 7892–7895. (b) Kleinman, L.; Bylander, D. M. *Phys. Rev. Lett.* **1982**, *48*, 1425–1428. (c) Hamman, D. R.; Schlüter, M.; Chiang, C. *Phys. Rev. Lett.* **1979**, *43*, 1494–1497.

(26) Fois, E.; Gamba, A.; Tabacchi, G. *J. Phys. Chem. A* **2009**, *113*, 15006–15015.

(27) Frisch, M. J.; et al. *Gaussian 03*, revision D.02; Gaussian, Inc.: Wallingford, CT, 2004.

(28) (a) Runge, E.; Gross, E. K. *Phys. Rev. Lett.* **1984**, *52*, 997–1000. (b) Casida, M. E.; Jamorsky, C.; Casida, K. C.; Salahub, D. R. *J. Chem. Phys.* **1998**, *108*, 4439–4449.

(29) Becke, A. D. *J. Chem. Phys.* **1993**, *98*, 5648–5652.

(30) (a) Figgen, D.; Rauhut, G.; Dolg, M.; Stoll, H. *Chem. Phys.* **2005**, *311*, 227–244. (b) Peterson, K. A.; Puzzarini, C. *Theor. Chem. Acc.* **2005**, *114*, 283–296.

(31) (a) Fois, E.; Gamba, A.; Tabacchi, G. *ChemPhysChem* **2005**, *6*, 1237–1239. (b) Fois, E.; Gamba, A.; Tabacchi, G. *ChemPhysChem* **2008**, *9*, 538–543.

(32) It should be stressed that no OPT_c-like structure was observed in the room-temperature trajectory, but it was built up by manual modeling, as a control.

(33) Liptay, W.; Weisenberger, H.; Tiemann, F.; Eberlein, W.; Konopka, G. *Z. Naturforsch.* **1968**, *23a*, 377–393.

(34) The $1n \rightarrow 1\pi^*$ transition, symmetry forbidden in gas-phase Fl (zero oscillator strength at 396 nm) is found very weak in OPT_a. Moreover, it is blue shifted at 297 nm because the stabilizing effect of K^+ on the Fl nonbonding 1n level, predominantly localized on O_{Fl}, is even larger than that on $1\pi^*$.

(35) Kleineks, P. W.; Ehresmann, J. O.; Nicholas, J. B.; Haw, J. F. *ChemPhysChem* **2006**, *7*, 114–116.

(36) Spanò, E.; Tabacchi, G.; Gamba, A.; Fois, E. *J. Phys. Chem. B* **2006**, *110*, 21651–21661.

(37) (a) Trudu, F.; Tabacchi, G.; Gamba, A.; Fois, E. *J. Phys. Chem. C* **2008**, *112*, 15394–15401. (b) Fois, E.; Gamba, A.; Trudu, F.; Tabacchi, G. *Nuovo Cimento* **2008**, *123B*, 1567–1474.

(38) Artioli, G.; Kvick, Å. *Eur. J. Mineral.* **1990**, *2*, 749–759.

(39) A binding energy of 25.3 kcal/mol has been obtained for the K^+/acetone pair (see the Supporting Information).

(40) Fois, E.; Gamba, A.; Spanò, E.; Tabacchi, G. *J. Mol. Struct.* **2003**, *644*, 55–66.

JP101635P